Resistivity Exponents in 3D Dirac Semimetals From Electron-Electron Interaction

Niklas Wagner,[1] Sergio Ciuchi,[2] Alessandro Toschi,[3] Björn Trauzettel,[4] and Giorgio Sangiovanni[4]
[1]Institut für Theoretische Physik und Astrophysik, Universität Würzburg, 97074 Würzburg, Germany
[2]Dipartimento di Scienze Fisiche e Chimiche, Università dell'Aquila, 67100 Coppito (AQ), Italy and Istituto dei Sistemi Complessi, CNR, 00185 Roma, Italy
[3]Institute of Solid State Physics, TU Wien, 1040 Vienna, Austria
[4]Institut für Theoretische Physik und Astrophysik and Würzburg-Dresden Cluster of Excellence ct.qmat, Universität Würzburg, 97074 Würzburg, Germany

(Received 18 December 2020; accepted 16 April 2021; published 20 May 2021)

We study the resistivity of three-dimensional semimetals with linear dispersion in the presence of on-site electron-electron interaction. The well-known quadratic temperature dependence of the resistivity of conventional metals is turned into an unusual T^6 behavior. An analogous change affects the thermal transport, preserving the linearity in T of the ratio between thermal and electrical conductivities. These results hold from weak coupling up to the nonperturbative region of the Mott transition. Our findings yield a natural explanation for the hitherto not understood large exponents characterizing the temperature dependence of transport experiments on various topological semimetals.

DOI: 10.1103/PhysRevLett.126.206601

Introduction.—Topologically protected nodal semimetals are characterized by a linear energy-momentum relation and can be viewed as a condensed-matter realization of Dirac and Weyl high-energy particles [1,2]. These materials possess peculiar transport properties as a result of their nontrivial electronic band structure and of conducting boundary modes. One of the most remarkable phenomena is the negative magnetoresistance of Weyl semimetals, a manifestation of the chiral anomaly [3,4]. The impact of impurity scattering on the conductivity of three-dimensional (3D) Dirac semimetals has attracted a lot of attention: a residual conductivity is found for short-range random potentials [5] but, at the same time, some of the universal transport features characterizing graphene emerge [6,7]. While for small disorder, propagating Dirac fermions determine the transport properties, localized states appear in the opposite limit giving rise to the non-Anderson scenario [8].

The low-energy spectrum of Dirac and Weyl nodes in three dimensions cannot be gapped out by any symmetry-preserving single-particle perturbation. Many-body effects, when dominant, lead instead to the breakdown of this protection and open a gap [9,10]. The energy-momentum dispersion and the density of states (DOS) of 3D Dirac semimetals are sketched in Fig. 1. The half-bandwidth D corresponds to an ultraviolet cutoff Λ on the momenta and sets the energy scale from which the physics becomes nonperturbative [11], eventually leading to a Mott transition of the Dirac cone.

In this Letter, we focus on the essential and, at the same time, simplest case of electron-electron interaction: a local intra-orbital Hubbard repulsion U. We investigate how the fundamental properties defining the electronic behavior of conventional conductors (such as the bulk diagonal thermal and electrical resistivity) get qualitatively modified in Dirac and Weyl semimetals. The results are compared to previous studies of the effects of impurity [6,12] and phonon [12] scattering as well as of long-range Coulomb interaction [7]. By combining analytical and nonperturbative numerical calculations, we unveil qualitative changes in the transport properties in the whole parameter regime, from small to large values of the dimensionless U/D coupling, where the Mott-Hubbard metal-insulator transition eventually occurs.

In the weak-coupling limit, we explicitly test the applicability to 3D Dirac semimetals of the Landau Fermi-liquid theory, which is based on a one-to-one correspondence between a system of interacting electrons and a gas of asymptotically free fermions. In Fermi liquids (FL), quasiparticle excitations are well defined if their characteristic

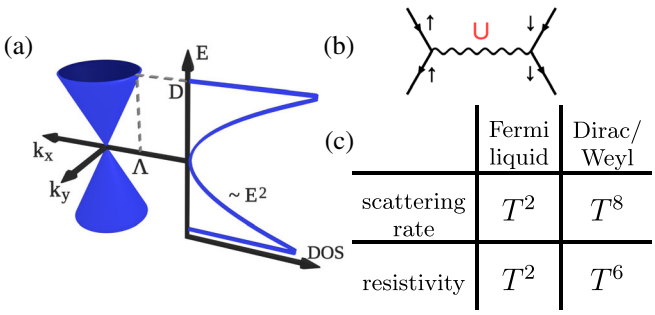

	Fermi liquid	Dirac/ Weyl
scattering rate	T^2	T^8
resistivity	T^2	T^6

FIG. 1. (a) Dirac or Weyl dispersion (for $k_z = 0$) and DOS with cutoff Λ in k space and energy half-bandwidth, indicated by D. (c) Temperature exponents for scattering rate and resistivity with Hubbard repulsion U, sketched in (b), comparing 3D Dirac or Weyl semimetals against conventional Fermi liquids.

energy is larger than their inverse lifetime, proportional to the scattering rate. If only electron-electron interaction is present the resistivity vanishes at zero temperature and grows as T^2. In 3D Dirac or Weyl semimetals, the DOS goes however quadratically to zero, approaching the Fermi level. This affects both the lifetime and the effective number of carriers available for transport leading to a characteristic and unexpected T^6 behavior for the resistivity ρ. Interestingly, even away from the neutrality point ($E = 0$), the power-law exponents remain fairly large (4 to 5) in a narrow though resolvable window of dopings. This observation has relevant implications for transport properties of Dirac or Weyl materials, such as WP_2, MoP, Cd_3As_2, as well as $Hg_{1-x}Cd_xTe$.

Weak-coupling result.—In the subspace of spin and orbital degrees of freedom, denoted by the Pauli matrices $\vec{S}$ and $\vec{\tau}$, respectively, the three-dimensional noninteracting Hamiltonian considered in Fig. 1 reads

$$H_0 = \hbar v S_z \otimes (\vec{k} \cdot \vec{\tau}), \tag{1}$$

where the momenta $\vec{k}$ live inside the sphere of radius Λ and v represents the velocity, i.e., the slope of the linear dispersion. The Hubbard U acts when the same orbital is occupied by two electrons with opposite spins; i.e., here we do not consider interorbital two-body terms [13]. In the weak coupling regime ($U \ll D$), perturbation theory holds and the scattering rate $\Gamma(\omega) = -\mathrm{Im}\Sigma(\omega)$ can be expressed as

$$\Gamma(\omega) \propto \frac{\pi V^3 U^2}{(\hbar v)^9} \int d\varepsilon_1 d\varepsilon_2 d\varepsilon_3 \delta(\omega + \varepsilon_1 - \varepsilon_2 - \varepsilon_3) \times (f_1(1-f_2)(1-f_3) + (1-f_1) f_2 f_3) \varepsilon_1^2 \varepsilon_2^2 \varepsilon_3^2, \tag{2}$$

where V is the volume of the unit cell, f_i indicates the Fermi-Dirac distribution function of ε_i and the cutoff has been set to infinity because of the weak-coupling condition. The quadratic behavior of the DOS enters explicitly in the integrand (last three factors) and cannot be considered constant any more, as in conventional metals. An analytic evaluation of (2) yields [13]

$$\Gamma(\omega) \propto \frac{8\pi V^3 U^2 T^8}{(\hbar v)^9} P_8(x), \tag{3}$$

where $x = \omega/T$ and $P_8(x) = x^8/8! + 7\pi^4 x^4/960 + 31\pi^6 x^2/1008 + 3\pi^8/128$, with T implicitly including the Boltzmann constant k_B. The first unexpected outcome of this simple calculation is therefore the much higher exponents entering the temperature and energy dependence of Γ, compared to the standard quadratic Fermi-liquid case [29].

Within the Kubo formalism we can compute the conductivity σ making use of our analytical result (3) for $\Gamma(\omega)$ and relying on the bubble approximation [30]. Calculations can be further simplified by disregarding the effect of the real part of the self-energy, as done in Ref. [5] and rewriting the conductivity in a Drude-Boltzmann fashion. This is achieved upon introducing the "$f\omega^2$" average of a quantity $\mathcal{Q}(\omega)$

$$\langle \mathcal{Q} \rangle_{f\omega^2} = \int d\omega \left[-\frac{\partial f}{\partial \omega} \right] \omega^2 \mathcal{Q}(\omega) / \underbrace{\int d\omega [-\frac{\partial f}{\partial \omega}] \omega^2}_{\mathcal{N}}, \tag{4}$$

which leads to the definition of an effective number density $n_{\mathrm{eff}}/m^* = \mathcal{N}/(6\pi^2\hbar^3 v)$ as well as a scattering time

$$\tau = \hbar \left\langle \frac{1}{2\Gamma(\omega)} + \frac{3\Gamma(\omega)}{2\omega^2} \right\rangle_{f\omega^2}. \tag{5}$$

Using these definitions, the conductivity assumes the simple Drude form:

$$\sigma = \frac{e^2 \tau n_{\mathrm{eff}}}{m^*}. \tag{6}$$

This Drude-like formulation allows us to disentangle the role of the DOS entering in the factor n_{eff}/m^* from that of the interaction, leading to a finite scattering time τ [31]. In conventional metals, the temperature dependence of σ stems entirely from τ, as all other quantities in Eq. (6) do not depend on T. In contrast, the parabolic DOS of the 3D Dirac semimetal results in a quadratic behavior of the effective number density: $n_{\mathrm{eff}}/m^* = T^2/(18\hbar^3 v)$. Using the polynomial expression of Γ given in Eq. (3) and considering that at low temperature the contribution of the second term in Eq. (5) is irrelevant, we arrive at $\tau \propto T^{-8}$. The resistivity calculated from Eq. (6), i.e., taking into account the temperature dependence of both n_{eff} and of τ, shows hence the characteristic $\rho \propto T^6$, shown in the Table of Fig. 1.

Beyond weak coupling.—By releasing the constraint $U \ll D$ and replacing perturbative analytic approaches with numerical many-body methods, we can access the intermediate-to-strong-coupling region. We do so using fully dressed dynamical mean field theory (DMFT) [32] Green's functions in the Kubo expression [13]. As an impurity solver, we use the iterated perturbation theory solver [33–36], which offers computational advantages maintaining a fair accuracy for our purposes [13]. The resistivity ρ as a function of T for different values of U and the corresponding exponent $\partial \log \rho / \partial \log T$ are shown in Fig. 2. For small U, where DMFT nicely reproduces our analytic results [green curves and blue dashed line in Fig. 2(a)] as well as approaching the Mott transition located at $U_c \approx 5.5D$, we find that ρ scales as T^6, in striking contrast with the T^2 resistivity of conventional metals. This particular behavior is not limited to low temperatures but remains visible up to $T \approx 0.1D$, as marked by the white region in the phase diagram in Fig. 2(b). The green region

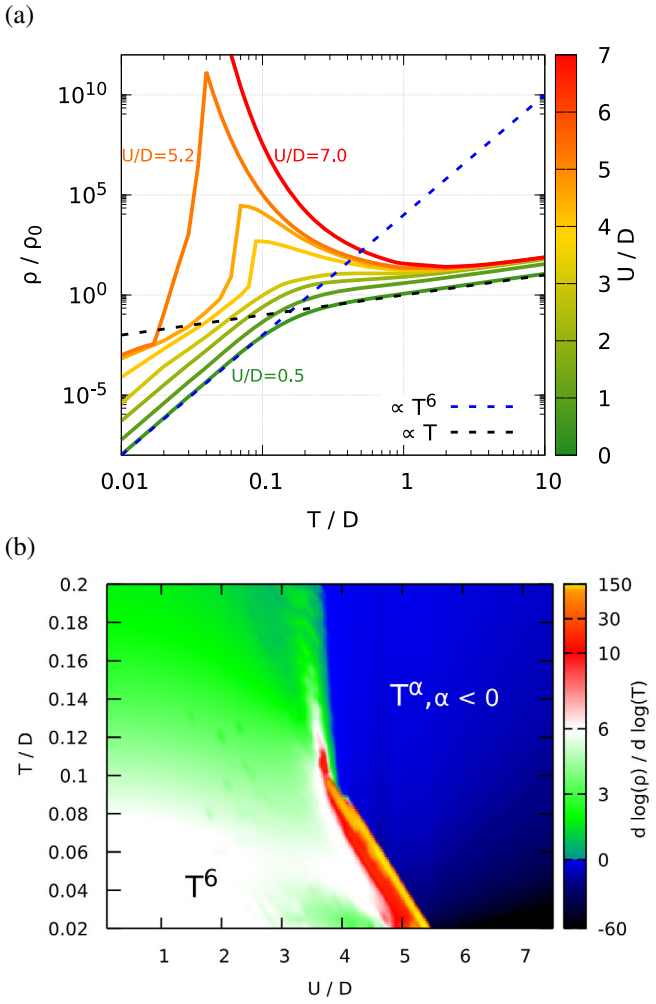

FIG. 2. (a) DMFT results for the resistivity ρ of a 3D Dirac or Weyl semimetal at zero doping, as a function of the temperature T for different values of the interaction strength U/D (color bar), in units of $\rho_0 = 6\pi^2\hbar^3 v/(e^2 D)$. The dashed lines indicate the asymptotic behavior for low temperature and weak coupling and for large temperature, respectively. (b) DMFT phase diagram, where the color indicates $\partial \log \rho / \partial \log T$, i.e., the exponent of the T dependence of ρ.

at low temperature around $U/D \approx 4$ reflects the presence of a low-energy kink in the T^6-resistivity behavior (see Ref. [13]). Upon further increasing T at $U < U_c$ the resistivity displays a smooth crossover to a linear regime [green lines in Fig. 2(a) and dark green region in Fig. 2(b)].

$\rho \propto T$ is usually associated to bad-metallic behavior, a phenomenon of high interest which can, however, have different physical origins. Here, its appearance is ascribed to incoherent high-temperature scattering, similar to what happens in systems with nonvanishing DOS at the Fermi level. For the case of a correlated metal on the Bethe lattice, the relation to the bad metallic regime of hydrodynamic theories [37,38] has been analyzed in detail in Ref. [39].

On the other side of the Mott transition instead, the typical exponential behavior of an insulating resistivity is recovered [red line in Fig. 2(a) and blue areas in Fig. 2(b)]. Close to the Mott transition the exponent becomes very large, in analogy with the results for a semicircular DOS [40]. The parameter region where $\rho \propto T^6$ holds is substantially larger than the corresponding T^2 one of conventional FL [40] (see Fig. S3 and Sec. IVe of the Supplemental Material [13]).

Finite doping.—After having found the T^{-6} dependence of the electrical conductivity, we examine how far this persists upon doping the Dirac semimetal ($\mu \neq 0$). Already a small doping adds contributions to the scattering rate with lower exponents, down to $T^2\mu^6$. For $\omega = 0$, an analytic calculation yields [13]

$$\Gamma(\omega = 0) \propto T^8 Q_6(y), \tag{7}$$

where now $y = \mu/T$ and $Q_6(y) = 3\pi^8 + 12\pi^6 y^2 + 20\pi^4 y^4 + 8\pi^2 y^6$. When the temperature scale is substantially smaller than the chemical potential, i.e., $T \lessapprox 0.2\mu(T)$, the thermal broadening is negligible and the Dirac point is sufficiently away in energy, such that it plays no role for transport properties. In this case, the T^2 term in Eq. (7) dominates and the scattering rate behaves similar to the usual FL. When T is increased beyond 0.2μ, the higher-order terms begin to contribute significantly. At $T > 0.6\mu$ [i.e., when the standard deviation of the derivative of the Fermi distribution ($\approx 1.8T$) is roughly equal to μ] the T^8 term prevails.

This is confirmed by a DMFT calculation of ρ away from the neutrality point, shown in Fig. 3. Upon increasing the temperature at $n = 0.5$ (dark blue circles), ρ goes from T^6 directly to T. With a small but finite doping, the conventional T^2 Fermi-liquid behavior emerges at low temperatures, in agreement with the analytical result (see Fig. 3).

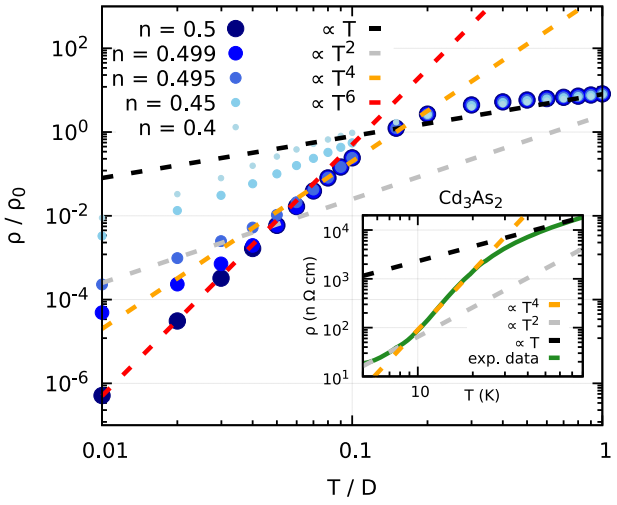

FIG. 3. DMFT results for the resistivity as a function of temperature of a Dirac semimetal for different fillings at interaction strength $U = 2D$. The inset shows experimental data for Cd_3As_2 from Ref. [41].

At larger temperatures, however, before crossing over to the linear behavior, higher T exponents in ρ are clearly visible. The extension of this intermediate region depends on the doping level. As we will discuss below, the possibility of realizing fast-growing (even though not necessarily a clean T^6) power-law resistivity can play a crucial role for the explanation of experiments on doped Dirac and Weyl semimetals. For larger deviations from half-filling the resistivity goes instead directly from quadratic to linear and the influence of the Dirac fermiology in the intermediate region is suppressed.

Other sources of scattering.—The precise way in which Γ depends on ω stems from the nature of the one- and two-body terms that we include in the model Hamiltonian. These can be, for instance, a random disorder potential, an electron-phonon interaction, as well as different parametrizations of the electron-electron repulsion, like the intra-orbital Hubbard U considered here.

Within the self-consistent Born approximation (SCBA), $\mathrm{Im}\Sigma$ arising from disorder is proportional to the DOS—hence it is quadratic in ω—and to the variance of the disorder distribution. As a consequence $\tau \propto T^2$. Interband transitions can be safely neglected. This way the temperature in the expression for σ drops out, yielding a residual resistivity at low T. The case of (a weak) electron-phonon interaction is similar, the only difference being an explicit (linear) temperature dependence appearing in the variance of the distribution of local displacements associated to classical phonons above the Debye temperature. This leads to $\tau \propto T^{-3}$ and, upon plugging this into Eq. (6), to $\sigma \propto 1/T$ which is in agreement with the high-temperature result described in Ref. [12]. A third situation which can be easily recasted in this simplified Drude-Boltzmann-like framework is a long-range Coulomb interaction at weak coupling strength: in this case, $\Gamma(\omega)$ is given by $\max(\omega, T)$ [6,7]. Interband contributions matter and one obtains $\tau \sim 1/T$ leading to $\sigma \propto T$ [13]. Having re-obtained these results makes the comparison of the various scattering mechanisms in three spatial dimensions easy. Vertex corrections may introduce modifications as it has been shown, for example, for Dirac fermions in 2D, where transport and quasiparticle scattering times get different T dependences [42].

Specific heat and thermal transport.—The dispersion of Dirac or Weyl semimetals affects also other important transport and thermodynamic coefficients. One relevant example is the temperature behavior of the specific heat. In contrast to the usual renormalized linear behavior of a conventional FL ($c_V \propto T/Z$, with Z being the quasiparticle weight) for the undoped Dirac semimetals it depends on the cube of the temperature ($c_V \propto T^3/Z^3$) [43]. Similar as for ρ, doping away from the degeneracy point introduces a conventional (linear) behavior at low temperatures: $c_V(T) \propto 7\pi^4 T^3/5Z^3(1+ay^2)$ with $y=\mu/T$ and $a=5Z^2/7\pi^2$. The crossover between FL-like and Dirac-like behavior happens at $T \approx 0.27Z\mu$, i.e., approximately the same temperature as for the scattering rate. We calculated the specific heat within DMFT using the approach outlined in Ref. [44]. The results confirm the trend given by the analytic expression [13].

Similarly, our DMFT calculations of the thermal conductivity yield results in sharp contrast to conventional FL: we find $\kappa \propto T^{-5}$. In analogy to $1/\sigma$ shown in Fig. 2(a), the thermal resistivity $1/\kappa$ displays a crossover at $T \sim 0.1D$, from T^5 to T^2. We can then conclude that the κ/σ ratio is linear in T at low temperatures, which represents a result compatible with a Wiedemann-Franz-type of relation. Let us recall that this conclusion holds roughly in the white region of the phase diagram of Fig. 2(b) and is reached within the bubble approximation for the conductivities [13].

Relation to materials.—First of all it is important to stress that, even though we have so far been explicitly referring to 3D Dirac semimetals, our results apply also to the case of Weyl nodes, since these are characterized by the same quadratic DOS. In the literature, high exponents for the resistivity have been reported in some Dirac and Weyl semimetals, e.g., in the type-II Weyl system WP_2 [45], in the multifold-fermion system MoP [46] and in the 3D Dirac semimetal Cd_3As_2 [41]. Data for the latter are shown in the inset to Fig. 3. As discussed above for the finite doping case, already a small distance between the Fermi energy and the Dirac point leads to the emergence of a conventional T^2 behavior for small T. Our results remain, however, applicable to the intermediate temperature region shown in Fig. 3, providing an interpretation for the observed T^4 behaviors of ρ without any *ad hoc* assumption. Despite the fact that the situation is more complicated for WP_2 and MoP due to the presence of additional bands, both compounds show similar behavior (see Ref. [13]), suggesting that the results of our simple model are at least qualitatively applicable to a wider range of materials. $Hg_{1-x}Cd_xTe$ has been reported as a realization of the so-called Kane semimetal [47], i.e., a 3D zero-gap Dirac system. Provided that the influence of the structural thermal expansion remains small, we expect the appearance of T^6 terms in the longitudinal resistivity. The situation at the critical doping, where the gap closes, is, however, disturbed by the presence of an additional flat band. The Weyl semimetal realized in compressively strained HgTe might offer a promising alternative, as it avoids the disturbance of the heavy-hole band and requires no fine-tuning of the doping [48].

Conclusions.—In three-dimensional Dirac and Weyl semimetals, the temperature power law of the scattering rate originating from short-range electron-electron interaction gains as many as *six* powers, compared to conventional FL. As a consequence, electrical and thermal resistivities are altered dramatically and go up *four* powers of T: in Dirac or Weyl systems we indeed find $\rho \propto T^6$ and $\kappa^{-1} \propto T^5$. These conclusions hold not only for weak

strengths of the Hubbard repulsion, where they can also be derived analytically, but also in a substantial region of the $T-U$ phase diagram, essentially up to the point at which the semimetal breaks down and is turned into a Mott insulator. These particular temperature exponents lead to an unusual situation: they describe a strongly suppressed contribution to transport from electron-electron repulsion at low temperatures but they rapidly prevail upon increasing T, in the intermediate-to-high regime. Interestingly, if we move away from the Dirac or Weyl point, the temperature exponent for the electrical resistivity is only slightly altered, shifting to $\rho \propto T^{4-5}$, offering a natural and simple explanation to the so far elusive origin of the high exponents of bulk diagonal transport coefficients measured in several Dirac and Weyl materials.

We thank D. Di Sante, H. Rostami and E. Cappelluti for useful conversations and Tian Liang for providing us with the original ρ vs T experimental data from Ref. [41] shown in Fig. 3. N. W., B. T., and G. S. are supported by the SFB 1170 Tocotronics, Funded by the Deutsche Forschungsgemeinschaft (DFG, German Research Foundation) Project-ID 258499086 and acknowledge financial support from the DFG through the Würzburg-Dresden Cluster of Excellence on Complexity and Topology in Quantum Matter *ct.qmat* (EXC 2147, project-id 390858490). We gratefully acknowledge the Gauss Center for Supercomputing e.V. for funding this project by providing computing time on the GCS Supercomputer SuperMUC at Leibniz Supercomputing Center. Computing time at HLRN (Berlin and Göttingen) is acknowledged. A. T. acknowledges financial support from the Austrian Science Fund (FWF), through the project I 2794-N35.

[1] N. P. Armitage, E. J. Mele, and A. Vishwanath, Weyl and Dirac semimetals in three-dimensional solids, Rev. Mod. Phys. **90**, 015001 (2018).
[2] T. Wehling, A. Black-Schaffer, and A. Balatsky, Dirac materials, Adv. Phys. **63**, 1 (2014).
[3] D. T. Son and B. Z. Spivak, Chiral anomaly and classical negative magnetoresistance of Weyl metals, Phys. Rev. B **88**, 104412 (2013).
[4] P. E. C. Ashby and J. P. Carbotte, Chiral anomaly and optical absorption in Weyl semimetals, Phys. Rev. B **89**, 245121 (2014).
[5] C. J. Tabert, J. P. Carbotte, and E. J. Nicol, Optical and transport properties in three-dimensional Dirac and Weyl semimetals, Phys. Rev. B **93**, 085426 (2016).
[6] A. A. Burkov, M. D. Hook, and L. Balents, Topological nodal semimetals, Phys. Rev. B **84**, 235126 (2011).
[7] P. Hosur, S. A. Parameswaran, and A. Vishwanath, Charge Transport in Weyl Semimetals, Phys. Rev. Lett. **108**, 046602 (2012).
[8] S. V. Syzranov and L. Radzihovsky, High-dimensional disorder-driven phenomena in Weyl semimetals, semiconductors, and related systems, Annu. Rev. Condens. Matter Phys. **9**, 35 (2018).
[9] T. Morimoto and N. Nagaosa, Weyl Mott insulator, Sci. Rep. **6**, 19853 (2016).
[10] V. V. Braguta, M. I. Katsnelson, A. Y. Kotov, and A. A. Nikolaev, Monte Carlo study of Dirac semimetals phase diagram, Phys. Rev. B **94**, 205147 (2016).
[11] T. Schäfer, G. Rohringer, O. Gunnarsson, S. Ciuchi, G. Sangiovanni, and A. Toschi, Divergent Precursors of the Mott-Hubbard Transition at the Two-Particle Level, Phys. Rev. Lett. **110**, 246405 (2013).
[12] S. Das Sarma, E. H. Hwang, and H. Min, Carrier screening, transport, and relaxation in three-dimensional Dirac semimetals, Phys. Rev. B **91**, 035201 (2015).
[13] See Supplemental Material at http://link.aps.org/supplemental/10.1103/PhysRevLett.126.206601 for additional information regarding the analytic and numerical regards presented in the main text and the comparison with experimental data, which also includes Refs. [14–28].
[14] M. Potthoff, T. Wegner, and W. Nolting, Interpolating self-energy of the infinite-dimensional Hubbard model: Modifying the iterative perturbation theory, Phys. Rev. B **55**, 16132 (1997).
[15] K. Byczuk, M. Kollar, K. Held, Y.-F. Yang, I. A. Nekrasov, T. Pruschke, and D. Vollhardt, Kinks in the dispersion of strongly correlated electrons, Nat. Phys. **3**, 168 (2007).
[16] A. Toschi, M. Capone, C. Castellani, and K. Held, Kinks in the Electronic Specific Heat, Phys. Rev. Lett. **102**, 076402 (2009).
[17] V. S. Oudovenko and G. Kotliar, Thermoelectric properties of the degenerate Hubbard model, Phys. Rev. B **65**, 075102 (2002).
[18] A. Khurana, Electrical Conductivity in the Infinite-Dimensional Hubbard Model, Phys. Rev. Lett. **64**, 1990 (1990).
[19] A. A. Abrikosov, L. P. Gor'kov, and I. E. Dzialoshinskii, *Methods of Quantum Field Theory in Statistical Physics*, rev. english ed. (Dover Publications, New York, 1975).
[20] I. Crassee, R. Sankar, W.-L. Lee, A. Akrap, and M. Orlita, 3D Dirac semimetal Cd_3 As_2: A review of material properties, Phys. Rev. Mater. **2**, 120302 (2018).
[21] C. Raas and G. S. Uhrig, Generic susceptibilities of the half-filled hubbard model in infinite dimensions, Phys. Rev. B **79**, 115136 (2009).
[22] A. Toschi, R. Arita, P. Hansmann, G. Sangiovanni, and K. Held, Quantum dynamical screening of the local magnetic moment in Fe-based superconductors, Phys. Rev. B **86**, 064411 (2012).
[23] N. Dasari, W. R. Mondal, P. Zhang, J. Moreno, M. Jarrell, and N. S. Vidhyadhiraja, A multi-orbital iterated perturbation theory for model Hamiltonians and real material-specific calculations of correlated systems, Eur. Phys. J. B **89**, 202 (2016).
[24] A. Galler, C. Taranto, M. Wallerberger, M. Kaltak, G. Kresse, G. Sangiovanni, A. Toschi, and K. Held, Screened moments and absence of ferromagnetism in FeAl, Phys. Rev. B **92**, 205132 (2015).
[25] A. Hausoel, M. Karolak, E. Sasioglu, A. Lichtenstein, K. Held, A. Katanin, A. Toschi, and G. Sangiovanni, Local magnetic moments in iron and nickel at ambient and earth's core conditions, Nat. Commun. **8**, 16062 (2017).

[26] C. Watzenböck, M. Edelmann, D. Springer, G. Sangiovanni, and A. Toschi, Characteristic Timescales of the Local Moment Dynamics in Hund's Metals, Phys. Rev. Lett. **125**, 086402 (2020).
[27] L. D. Re and A. Toschi, The dynamical vertex approximation for many-electron systems with spontaneously broken su(2)-symmetry, arXiv:2011.04080.
[28] K. Held, R. Peters, and A. Toschi, Poor Man's Understanding of Kinks Originating from Strong Electronic Correlations, Phys. Rev. Lett. **110**, 246402 (2013).
[29] P. Coleman, *Introduction to Many Body Physics* (Cambridge University Press, New York, NY, 2015).
[30] Restricting to the bubble diagram does not represent a too severe approximation in our case, as we are going to compute the conductivities of these 3D semimetals within dynamical mean-field theory and with an intra-orbital-only Hubbard interaction, for which the vanishing of vertex corrections in ladder diagrams can be explicitly demonstrated [13]. Adding interorbital two-body terms would instead generate vertex corrections to the current-current response, similarly to what occurs for disorder or electron-phonon interaction.
[31] Note that m^* is equal to m if one makes exactly the same approximations as in Ref. [5]; however, the formulas given here are more general since one can in principle include the effects of the real part of the self-energy via m^*.
[32] A. Georges, G. Kotliar, W. Krauth, and M. J. Rozenberg, Dynamical mean-field theory of strongly correlated fermion systems and the limit of infinite dimensions, Rev. Mod. Phys. **68**, 13 (1996).
[33] A. Georges and G. Kotliar, Hubbard model in infinite dimensions, Phys. Rev. B **45**, 6479 (1992).
[34] M. J. Rozenberg, G. Kotliar, and X. Y. Zhang, Mott-Hubbard transition in infinite dimensions. II, Phys. Rev. B **49**, 10181 (1994).
[35] H. Kajueter, G. Kotliar, and G. Moeller, Doped Mott insulator: Results from mean-field theory, Phys. Rev. B **53**, 16214 (1996).
[36] H. Kajueter and G. Kotliar, New Iterative Perturbation Scheme for Lattice Models with Arbitrary Filling, Phys. Rev. Lett. **77**, 131 (1996).
[37] A. Lucas and S. A. Hartnoll, Resistivity bound for hydrodynamic bad metals, Proc. Natl. Acad. Sci. U.S.A. **114**, 11344 (2017).
[38] S. A. Hartnoll, Theory of universal incoherent metallic transport, Nat. Phys. **11**, 54 (2015).
[39] N. Pakhira and R. H. McKenzie, Absence of a quantum limit to charge diffusion in bad metals, Phys. Rev. B **91**, 075124 (2015).
[40] J. Vučičević, H. Terletska, D. Tanasković, and V. Dobrosavljević, Finite-temperature crossover and the quantum Widom line near the Mott transition, Phys. Rev. B **88**, 075143 (2013).
[41] T. Liang, Q. Gibson, M. N. Ali, M. Liu, R. J. Cava, and N. P. Ong, Ultrahigh mobility and giant magnetoresistance in the Dirac semimetal Cd_3As_2, Nat. Mater. **14**, 280 (2015).
[42] E. Cappelluti and L. Benfatto, Vertex renormalization in dc conductivity of doped chiral graphene, Phys. Rev. B **79**, 035419 (2009).
[43] H.-H. Lai, S. E. Grefe, S. Paschen, and Q. Si, Weyl Kondo semimetal in heavy-fermion systems, Proc. Natl. Acad. Sci. U.S.A. **115**, 93 (2018).
[44] G. Rohringer and A. Toschi, Impact of nonlocal correlations over different energy scales: A dynamical vertex approximation study, Phys. Rev. B **94**, 125144 (2016).
[45] N. Kumar, Y. Sun, N. Xu, K. Manna, M. Yao, V. Süß, I. Leermakers, O. Young, T. Förster, M. Schmidt, H. Borrmann, B. Yan, U. Zeitler, M. Shi, C. Felser, and C. Shekhar, Extremely high magnetoresistance and conductivity in the type-II Weyl semimetals WP_2 and MoP_2, Nat. Commun. **8**, 1642 (2017).
[46] N. Kumar *et al.*, Extremely high conductivity observed in the triple point topological metal MoP, Nat. Commun. **10**, 2475 (2019).
[47] M. Orlita, D. M. Basko, M. S. Zholudev, F. Teppe, W. Knap, V. I. Gavrilenko, N. N. Mikhailov, S. A. Dvoretskii, P. Neugebauer, C. Faugeras, A.-L. Barra, G. Martinez, and M. Potemski, Observation of three-dimensional massless Kane fermions in a zinc-blende crystal, Nat. Phys. **10**, 233 (2014).
[48] D. M. Mahler, J.-B. Mayer, P. Leubner, L. Lunczer, D. Di Sante, G. Sangiovanni, R. Thomale, E. M. Hankiewicz, H. Buhmann, C. Gould, and L. W. Molenkamp, Interplay of Dirac Nodes and Volkov-Pankratov Surface States in Compressively Strained HgTe, Phys. Rev. X **9**, 031034 (2019).